Morphological characterization of a new low-bandgap thermocleavable polymer showing stable photovoltaic properties

Journal:	*Journal of Materials Chemistry A*
Manuscript ID	TA-ART-05-2016-004321.R1
Article Type:	Paper
Date Submitted by the Author:	08-Jun-2016
Complete List of Authors:	Vahdani, Pierayeh; Simon Fraser University, Department of Physics Li, Xianzhen; Simon Fraser University, Department of Chemistry Zhang, Chi; Simon Fraser University, Department of Chemistry Holdcroft, Steven; Simon Fraser University, Department of Chemistry Frisken, Barbara ; Simon Fraser University, Physics

SCHOLARONE™
Manuscripts

Morphological characterization of a new low-bandgap thermocleavable polymer showing stable photovoltaic properties

Pierayeh Vahdani,[a] Xianzhen Li,[b] Chi Zhang,[b] Steven Holdcroft[b] and Barbara J. Frisken[a,]*

[a]Department of Physics and [b]Department of Chemistry, Simon Fraser University, 8888 University Drive, Burnaby, BC, V5A 1S6, Canada

* Corresponding author; *E-mail address*: frisken@sfu.ca

Abstract

The stability of the morphology of bulk heterojunction photovoltaic cells employing a novel low-bandgap polymer as donor is studied. The polymer is based on a thieno[3,4-b] thiophene benzo[1,2-b:4,5-b']dithiophene (PTB) backbone with tetrahydropyranyl (THP) side chains that are cleaved upon thermal treatment, which leads to stable performance of the photovoltaic properties during an accelerated aging process achieved by thermal annealing. The morphology of films made from blends of the polymer with PCBM is investigated before (PTB(THP):PCBM) and after (dPTB:PCBM) cleaving at micro and nanoscale using optical microscopy, transmission electron microscopy, and grazing incidence small angle x-ray scattering. Results are compared to films made from blends of poly(3-hexylthiophene) (P3HT:PCBM) and the version of the PTB series whose monomer is closest to that of PTB(THP), PTB4 (PTB4:PCBM). All three techniques demonstrate that phase separation is suppressed at the micro and nanoscale in the dPTB:PCBM films, while large micron-sized PCBM aggregates develop during thermal annealing in P3HT:PCBM, PTB4:PCBM and PTB(THP):PCBM films. Our studies show that the removal of THP-terminated side chains can lead to stable morphology, and result in stable performance of photovoltaic cells. While we have focused on comparison to PTB4 blends, our results should be transferable to other polymers in the PTB series.

1. Introduction

Bulk heterojunction (BHJ) solar cells based on a blend of conjugated polymers, as the electron donor, and a fullerene derivative such as phenyle butyric acid methyl ester (PCBM), as the electron acceptor, are considered to be promising candidates for renewable energy thanks to low manufacturing costs and easy processability. The registered power conversion efficiency (PCE) of a single junction BHJ solar cell is now approaching 11%.[1] Despite considerable improvements in the PCE of these devices, the long term stability is still sub-optimal for successful commercialization.[2,3] In an ideal BHJ solar cell, electron donor and electron acceptor materials form a network consisting of phase-separated domains of donor and acceptor. The size of the domains should be small enough to provide large enough interfacial area for efficient exciton dissociation and short enough separation to prevent recombination. Domains should form percolating pathways for separated electrons and holes to reach opposite electrodes. The initial morphology of the photoactive layer in BHJ solar cells is mainly influenced by the thermodynamics of the blend and the kinetics of film formation.[4-6] This morphology is kinetically unstable and moves towards a more stable state after the film is formed. Consequently, phase separated domains in the device gradually grow larger, resulting in the discontinuity of the network, and leading directly to the loss of PCE and device degradation. In particular, the formation of micron-sized PCBM aggregates has been visualized previously upon prolonged thermal annealing, which simulates the aging process. Various factors, such as the crystallinity of the donor polymer, the choice of solvent and the annealing conditions, have been shown to influence the size and shape of PCBM aggregates. [7-10]

Several strategies have been employed to improve morphological stability in the active layer of BHJ solar cells. Block copolymers combining conjugated polymer and fullerene derivatives together as a single component material were one of the first solutions suggested.[11] This idea, however, was not entirely successful due to the complex synthetic process involved and low solubility of fullerene.[3] Another approach is to incorporate functionalized crosslinkable units either within the main polymer chain or in the side chains. Upon functionalization of these units the initial morphology can be locked in.[12,13] A third approach is to design thermo-cleavable polymers, where side chains can be removed after processing, rendering them insoluble. Incorporating side chains that can be removed or shortened after the film is formed rigidifies the backbone and suppresses the macro-phase separation.[14-16] Apart from the

consideration of enhanced stability, the design of tandem organic solar cells,[17] consisting of a stack of multiple active layers, requires active layers that do not dissolve while casting the new layers on top. Thus, thermocleavable polymers are potential candidates in manufacturing tandem organic cells as well.

In this work, we have investigated the morphology of a novel polymer that consists of thermocleavable side chains grown onto a thieno[3,4-b]thiophenebenzodithiophene (PTB) backbone, shown in Figure 1(a). Low-bandgap polymers built on the PTB backbone have been shown to achieve PCEs of up to 9.2%, where the PCE achieved depends on the nature of the side chain, whether the acceptor is $PCBM_{61}$ or $PCBM_{71}$, the solvents used in casting the film, and device engineering.[18] Morphological studies associate their high performance with an ideal morphology of the donor–acceptor network that allows the intercalation of PCBM molecules among the polymer chains.[19] The morphology of PTB7, one of the most promising versions of this polymer, does degrade when samples are thermally annealed; others have shown that it is possible to stabilize the morphology by crosslinking the acceptor fullerene[20] or by light-induced oligomerization of $PC_{60}BM$.[21]

Our samples consist of tetrahydropyranyl (THP) side chains attached to a low-bandgap PTB polymer to form PTB(THP). The monomer on which PTB(THP) is built is most similar to that of PTB4; the monomers under study are compared in Figure 1(a). The PTB4 monomer consists of alternating thienothiophene and benzodithiophene units on its backbone.[22] There is an n-octyl side chain attached to the thienothiophene unit and the remaining aromatic proton on the thienothiophene unit is replaced by fluorine. A pair of 2-ethylhexyloxy sidechains are attached to the benzodithiophene units. In PTB(THP), the 2-ethylhexyloxy sidechains are replaced by THP side chains. The THP attachment is cleaved upon thermal treatment to yield deprotected PTB(THP) or dPTB. When used as the active layer in a photovoltaic device, we find that this results in greater stability of photovoltaic properties. To test whether this can be attributed to the stability of the morphology, we have used imaging and scattering techniques to study the morphology during thermally-induced aging. Imaging techniques of optical microscopy and transmission electron microscopy (TEM) have been employed to investigate the development of phase separation at macroscopic and sub-microscopic length scales. These studies have been complemented by grazing incidence small-angle x-ray scattering (GISAXS) to obtain information averaged over areas comparable to the size of the PV devices. Results for

active layers consisting of PTB4:PCBM, PTB(THP):PCBM and dPTB:PCBM films, making comparison to changes in the well-studied P3HT:PCBM system, are reported.

2. Results and Discussion

2.1. Polymer Properties and Device Characteristics

Synthetic routes for the monomers and polymers investigated in this work are outlined in Scheme 1, Supporting Information. The chemical structures of PTB, PTB4, PTB(THP), and dPTB polymers are shown in Figure 1 (a). Data from thermogravimetric analyses (TGA) of pristine PTB(THP) and PTB-THP containing camphor sulfonic acid (CSA) (5 mol-% based on the THP unit) are shown in Figure 1 (b). The observed mass losses are 20 wt% for pristine PTB(THP) and 19.5 wt% in the presence of CSA, where CSA serves as an acidic catalyst. The THP functionality is calculated to be 21.3 wt% of PTB(THP) which confirms the loss in mass is due to thermolytic cleavage of the THP group and elimination of dihydropyran.[23,24] It can also be seen in Figure 1 (b) that the onset temperature required to remove THP groups from PTB(THP) decreases from 210 °C to 140 °C in the presence of a catalytic amount of CSA. FTIR spectra of the polymer before and after thermal treatment at 150 °C in the presence of CSA also confirms the cleavage of THP attachment upon heating (Figure S1, Supporting Information). PTB(THP) is highly soluble in common solvents, such as tetrahydrofuran (THF), chloroform, dichloromethane, toluene, chlorobenzene, and dichlorobenzene. However, after removal of the THP, the resulting film is no longer soluble in common solvents except in THF and N,N-dimethylformamide (DMF).

Differential scanning calorimetry (DSC) scans (Figure S2, Supporting Information), show a reversible transition at around 185 °C, which we attribute to the glass transition of the polymer (bulk sample). The first scan also shows a prominent endothermic peak at 270 °C which correlates with the removal of the THP groups by thermolytic cleavage (deprotection) observed in TGA. In the second scan, the deprotection peak is no longer observed, confirming the completion of the deprotection process. From the 10 °C heating rate of the experiment, we find that the deprotection of the 3.45 mg sample finished in 2.2 minutes. The glass transition temperature T_g remained the same after deprotection, indicating the deprotection process did not significantly change the physical properties of the polymer. This is also evidenced by UV-vis absorption spectra of PTB-THP polymer films, before and after deprotection, as well as films cast from PTB(THP):PCBM, and dPTB:PCBM blends, before and after deprotection, which

show only a small (2-5%) decrease in absorption after deprotection (Figure S3, Supporting Information).
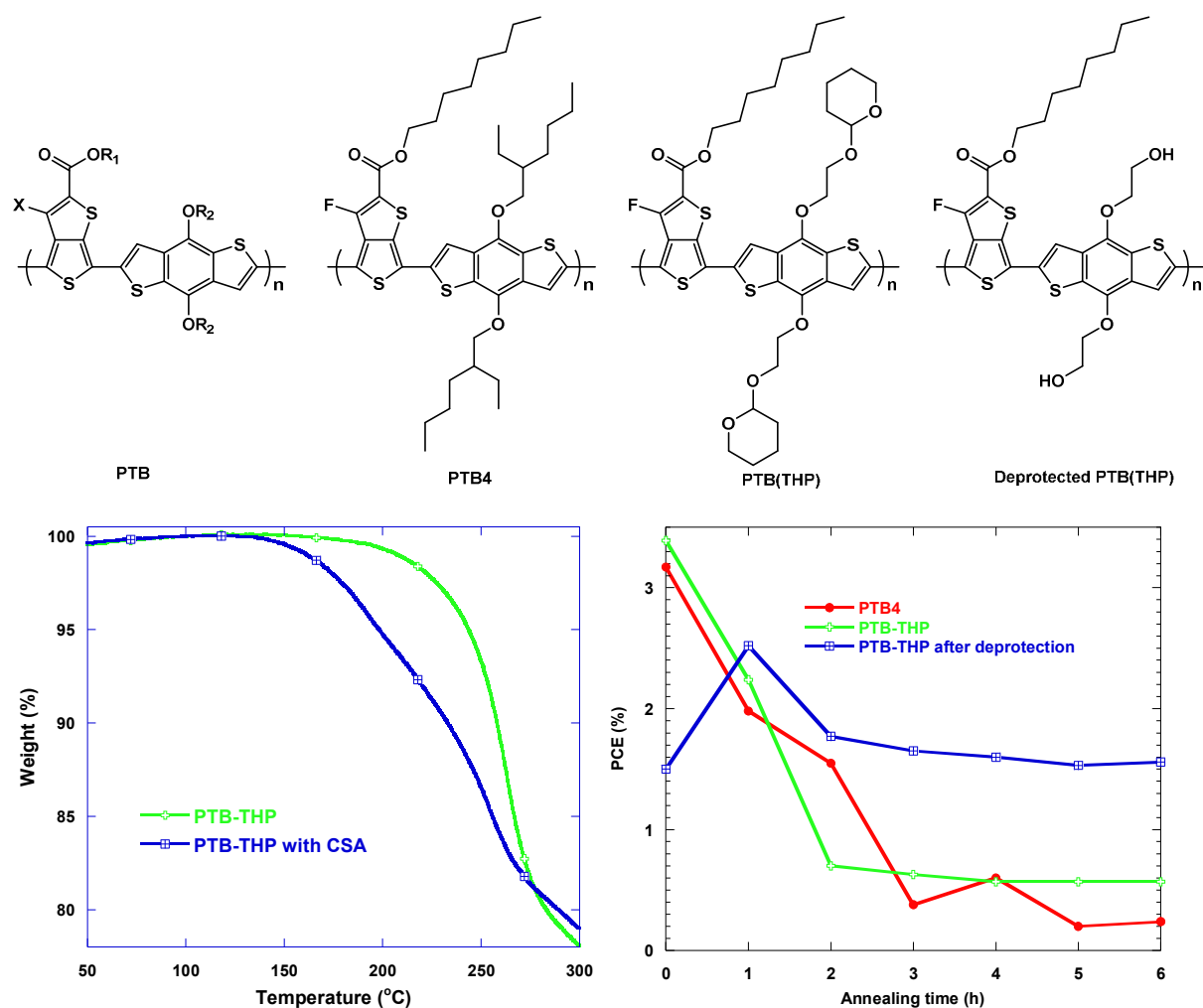

Figure 1. Chemical structures of PTB, PTB4, PTB(THP), and deprotected PTB(THP) (dPTB) polymers as well as results of (b) thermogravimetric analysis of PTB-THP with (blue) and without (green) 5 mol % of camphor sulfonic acid (CSA). The final panel, (c), shows PCEs of photovoltaic devices with active layers consisting of PTB4:PC$_{61}$BM, PTB(THP):PC$_{61}$BM and dPTB:PC$_{61}$BM as a function of annealing time at 130 °C.

Solar cell devices were fabricated based on the conventional configuration of ITO/PEDOT:PSS/Polymer:PC$_{61}$BM/Ca/Al with a polymer:PCBM ratio of 1:1 in wt%. To simulate the aging process, devices made from PTB4:PCBM, PTB(THP):PCBM, and dPTB:PCBM blends were annealed in a nitrogen glove-box and characterized every hour for up

to 6 hr. All dPTB:PCBM samples were initially annealed at 130 °C in the presence of CSA for an extra 5 min to be deprotected (converted from PTB(THP):PCBM+5 mol% CSA to dPTB:PCBM).

The change in the PCE of solar cells made from all the three polymers blended with PCBM are plotted in Figure 1 (c) as a function of annealing time (for further details, see Table 1 and Figure S4, Supporting Information). The efficiency degraded dramatically from 3.2% to 0.2% for PTB4:PCBM and from 3.4% to 0.6% for the PTB(THP):PCBM after 6 hr of annealing while, despite the lower starting value for dPTB:PCBM, its efficiency remains quite stable after 6 hr of annealing. The lower starting efficiency obtained for dPTB:PCBM compared to PTB4:PCBM and PTB(THP):PCBM can be attributed to the deprotection process, which requires 5 min of annealing. After the first hour of annealing, the photovoltaic performance was improved with a PCE value of 2.5%. The external quantum efficiency (EQE) curves show an increase in EQE of dPTB:PCBM after an hour of annealing, after which it remains stable (Figure S5, Supporting Information) compared to the EQE for PTB(THP):PCBM and PTB4:PCBM which drops after annealing, demonstrating the photovoltaic stability of the dPTB:PCBM devices. From cyclic voltammetry (Figure S6, Supporting Information), the HOMO and LUMO levels of PTB(THP) are found at -4.9 eV and -3.4 eV respectively, corresponding to a bandgap of 1.5 eV, which is consistent with the optical bandgap of 1.57 eV found through UV-vis spectroscopy. The added ether groups on the sidechain may have contributed to the high HOMO level compared to PTB4 (-5.12 eV). The higher HOMO level also explains the relatively low open circuit voltage (Voc) found in PV measurements, since Voc is related to the energy level difference between the HOMO of the polymer and the LUMO of the PCBM.[25]

2.2. Morphology of the active layer

We used optical microscopy to obtain a qualitative understanding of the morphology of the active layer at length scales ranging from 1-100 μm. Figure 2 shows results from reflection-mode microscopy for the samples prepared for GISAXS measurements: (a-d) P3HT:PCBM, (e-h) PTB4:PCBM, (i-l) PTB(THP):PCBM, and (m-p) dPTB:PCBM. In this figure, the columns represent samples aged at 130 °C for different times: 0, 1, and 6 hr.
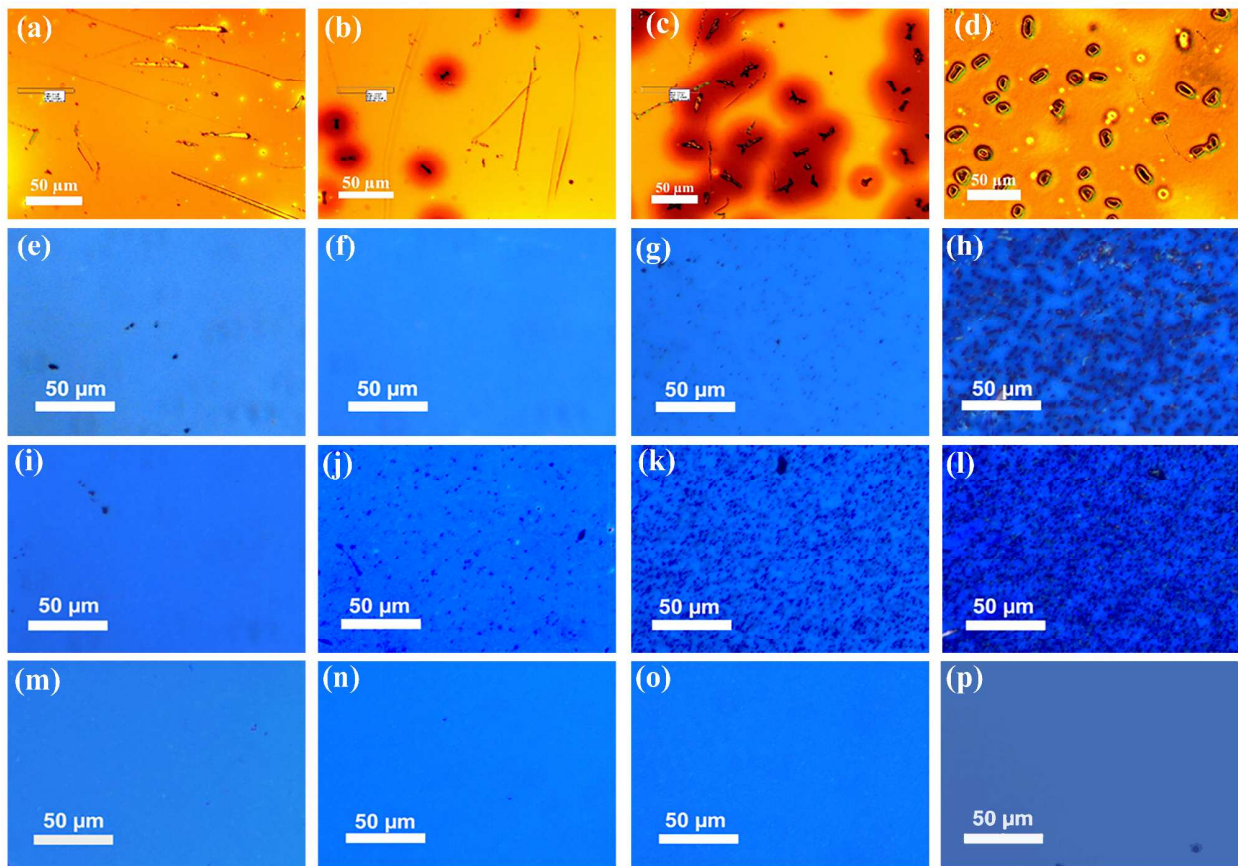
Figure 2. Optical microscopy images for films of (a-d) P3HT:PCBM, (e-h) PTB4:PCBM, (i-l) PTB(THP):PCBM, and (m-p) dPTB:PCBM. The films have been aged at 130 ^{o}C for 0 hr (a, e, i, m), 1 hr (b,f,j,n), 3 hr (c,g,k,o), and 6 hr (d,h,l,p). The bars indicate a scale of 50 μm.

Optical microscopy indicates that macroscopic phase separation is suppressed in the dPTB:PCBM films. P3HT:PCBM, PTB4:PCBM and PTB4:PCBM samples show the presence of dark aggregates that grow and increase in size as aging time increases, but these aggregates are absent in the sample containing the thermally cleaved polymer, dPTB:PCBM. The dark aggregates are due to high concentrations of PCBM. PCBM aggregates of about 10 μm in size are formed in P3HT:PCBM (Figure 2, a-d) after an hour of aging and grow in number and in size during 6 hr of aging, consistent with results of others.[26,27] In PTB4:PCBM films, aggregates start to appear after 3 hr of aging but they grow quickly resulting in structures varying in size and shape from ~ 1μm aggregates to ~ 4μm needle-like aggregates within 6 hr (Figure 2, e-h). Similar to P3HT:PCBM, aggregates appear in the PTB(THP):PCBM films after an hour of aging (Figure 2, i-l) and, while their number increases during six hours of annealing, the size of the

aggregates does not change significantly. Note that some differences in aggregate growth may be due to the fact that PTB4:PCBM films are cast from DCB, while P3HT:PCBM, PTB(THP):PCBM and dPTB:PCBM films are cast from chloroform:DCB mixtures, as it is known that PCBM has a lower solubility in chloroform than DCB.[28] In contrast to P3HT:PCBM, PTB4:PCBM, and PTB(THP):PCBM films, micron size aggregates are not observed in dPTB:PCBM films (Figure 2, m-p) even after 6 hr of aging.

A closer look at the optical microscopy data suggests a good correlation between PCE measurements (Figure 1) and the macro-phase separation behavior of these samples. The drop in efficiency of the PTB4:PCBM and PTB(THP):PCBM films after several hours of annealing is correlated with the early appearance of micron-sized PCBM aggregates. The efficiency continues to deteriorate after 3 hr as a result of more drastic growth in the size or number of the aggregates.

To obtain insight into the phase behavior of the films at smaller length scales we have also performed TEM and GISAXS measurements. Figure 3 shows TEM observations of as-cast and aged samples (0 to 6 hr) for different polymer films. Due to its higher electron density compared to the polymers, PCBM scatters the electron beam more strongly. As a result, darker regions in the TEM images signify PCBM-rich domains.[29] The TEM images feature three different structures. Large-scale (> 200 nm) PCBM aggregates are observed in the P3HT:PCBM, PTB4:PCBM and PTB(THP):PCBM films at aging times consistent with results from optical microscopy. No large-scale PCBM aggregates are observed in the dPTB:PCBM films. Overall the PTB blend films show a more uniform background structure than P3HT:PCBM in TEM images, suggesting that PCBM is more miscible in these polymers. PTB4:PCBM films also show densely-packed PCBM aggregates about 10-20 nm in size that start to form after 5 minutes of
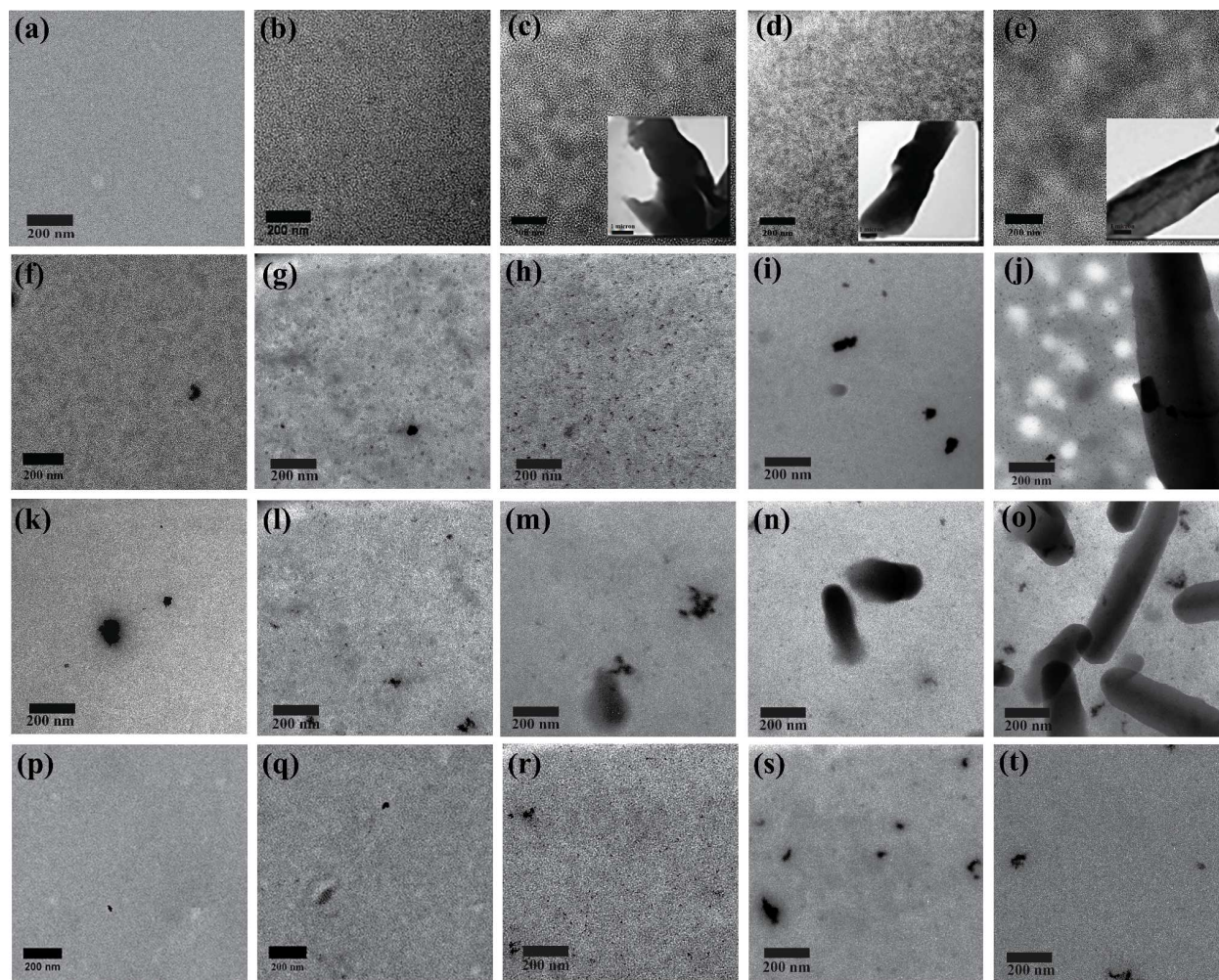
Figure 3: Bright field TEM images of a) P3HT: PCBM as cast (a) and aged for 0, 1, 3 and 6 hours (b-e), PTB4: PCBM as cast (f) and aged for 0, 1, 3 and 6 hrs (g-j), PTB(THP):PCBM as cast (k) and aged for 0, 1, 3, and 6 hrs (l-o), and dPTB:PCBM as cast (p) and aged for 0, 1, 3 and 6 hrs (q-t). The scale bar in the insets for (c), (d) and (e) is 1 μm.

annealing (Figure 3, g-j). These aggregates remain with no significant change in size, shape or population during aging while formation of micron-sized PCBM aggregates appear (Figure 3, i-j). Some of the TEM images reveal low-contrast structure at 100-200 nm particularly in all of the P3HT:PCBM samples (Figure 3, a-e), in the as-cast and 0 hr samples of PTB4:PCBM (Figure 3, f-g). The structure resembles a weakly-phase separated domain structure. This domain structure has been reported previously for P3HT:PCBM[29] films and for various PTB:PCBM films.[22] These weakly phase-separated domains are less obvious in PTB(THP):PCBM and dPTB:PCBM.

Finally, there is some evidence of undissolved PCBM aggregates, particularly in the as-cast sample of PTB(THP):PCBM (Figure 3, k). As seen in optical microscopy images, the TEM images confirm PCBM aggregation in P3HT:PCBM, PTB4:PCBM and PTB(THP):PCBM samples, and that no aggregation occurs in dPTB:PCBM samples. They also confirm the difference in rate of aggregation, with PCBM aggregation starting within one hr of aging in P3HT:PCBM and PTB(THP):PCBM films but not appearing until after 3 hr of aging in the PTB4:PCBM films. We attribute this to use of different solvents, as mentioned previously.

We carried out GISAXS measurements on all of the films shown in Figure 2 to study the nanoscale behavior of the morphology further. The data obtained by integrating along a horizontal line of the 2D GISAXS images are presented in Figure 4. Examples of 2D GISAXS data for samples annealed for 0 and 6 hr are shown in Figure S7, Supporting Information. Figure S8, Supporting Information, shows a sample 2D GISAXS pattern, the region selected for integration as well as the associated integrated data.
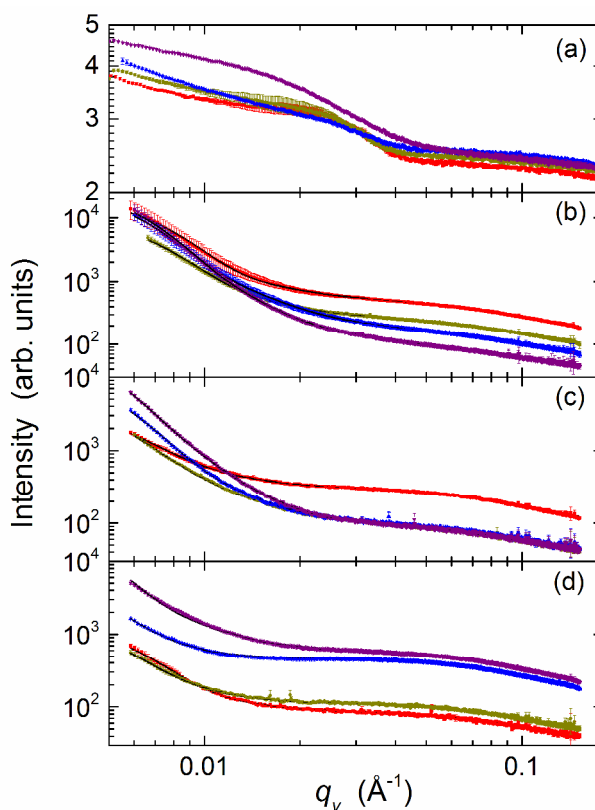

Figure 4. The integrated data from 2D GISAXS images of (a) P3HT:PCBM, (b) PTB4:PCBM, (c) PTB(THP):PCBM, and (d) dPTB:PCBM films annealed for 0 hr (■), 1 hr (●), 3 hr (▲), and 6 hr (▼) at 130 °C. Curves in (b)-(d) are fits of Eq. 1 to the data.

The data for all of the PTB blend films, presented in Figure 4, show a broad bump at mid-high q-range (0.02 - 0.1 Å^{-1}) with an upturn in the low-q region (q < 0.02 Å^{-1}). In the PTB4:PCBM and PTB(THP):PCBM samples, the broad bump decreases in intensity as the annealing time increases. The bump indicates presence of small (2 nm) domains within the polymer matrix. As the bump decreases in amplitude, the low-q upturn becomes more pronounced, consistent with the formation of larger aggregates as the samples age. There are differences in the behavior of the two samples; the amplitude of the bump decreases gradually for the PTB4:PCBM samples, and more abruptly for the PTB(THP):PCBM samples. On the other hand, the dPTB:PCBM samples show an increase in the amplitude of the bump with little change in the low-q behavior until the end of the aging process. P3HT:PCBM thin films aged for 0 and 1 hr show a shoulder at mid q-range (0.015-0.06 Å^{-}1), which disappears as aging time increases. This shoulder has been attributed to the formation of PCBM clusters in the blend, which dissolve over time and form large PCBM aggregates.[30-32] Modeling of our data for P3HT:PCBM films[33] reveals that the size of the aggregates remains constant at about 8 nm during the first 3 hr of aging and increases to 16 nm after 6 hr of aging. The volume fraction of the aggregates increases with aging indicating more aggregates are being formed as a result of the aging process. The polydispersity is large and remains almost constant during the process.

To further analyze the GISAXS experimental data for the PTB polymer blends, we fit a unified model that uses a combination of Porod's and Guinier's laws to describe the morphology at different structural levels to the data[34]

$$I(q) = G_1 \exp\left(-q^2 R_{g1}^2 / 3\right) + B \exp\left(-q^2 R_{g2}^2 / 3\right)\left(\frac{1}{q_1^*}\right)^P + G_2 \exp\left(-q^2 R_{g2}^2 / 3\right) + A \quad , \quad (1)$$

where P is the Porod scaling factor, R_{gi} are the radii of gyration, and Gi, B, and A are amplitudes of the four terms. The first and second terms describe the low-q data in terms of a length scale R_{g1} and a mass-fractal regime characterized by fractal dimension P. The third term describes the bump at high-q in terms of a length scale R_{g2}. The parameter q_1^* is part of the bridging between these two regimes and is given by

$$q_1^* = \frac{q}{\left[\operatorname{erf}(kqR_{g1} / \sqrt{6})\right]^3} \quad , \quad (2)$$

11

where k is an empirical constant defined in Ref. [34]. The Irena package[35] was used to fit the model function to the data. This model provides a good fit to the data and results are shown as solid curves in Figure 4.

Values for R_{g2} and G_2 are shown in Figures 5 (a) and (b), respectively. The results for the Guinier regime at high-q indicate that small aggregates ranging from 1.7 to 2.2 nm are present in all PTB samples. This is consistent with the picture of well-mixed donor and acceptor phases within the film. These aggregates are significantly smaller than the aggregates observed in the P3HT:PCBM samples indicating that better mixing is obtained in this polymer blend. These regions grow slightly in size in the PTB4:PCBM samples with aging, but the size of these regions is roughly constant in the PTB(THP):PCBM and dPTB:PCBM samples. The amplitude of this term indicates that the impact of these aggregates on the scattering is decreasing during aging for the PTB4 and PTB(THP) blends, but increasing for the dPTB blends. This could be due to a change in contrast between the aggregates and the polymer, or due to an increase in the number of aggregates.
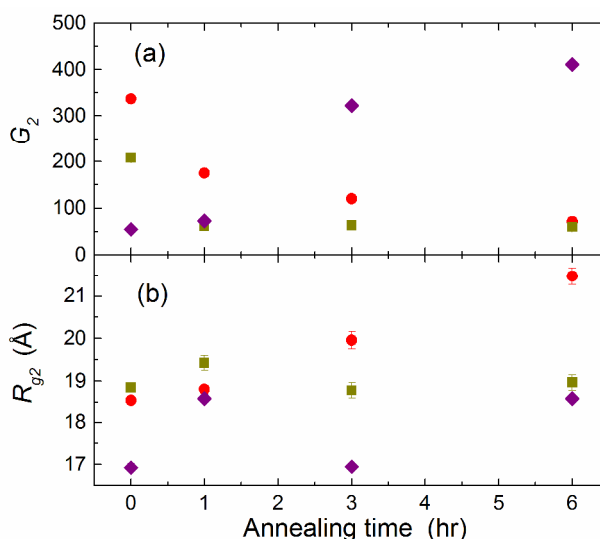

Figure 5. Values for high-q fitting coefficients: amplitude (G_2) and radius of gyration (R_{g2}) obtained by fitting Eq. 1 to the GISAXS data for the PTB blends shown in Figure 4 as a function of aging time simulated by thermal annealing: (●) PTB4:PCBM, (■) PTB(THP):PCBM, and (♦) dPTB:PCBM.
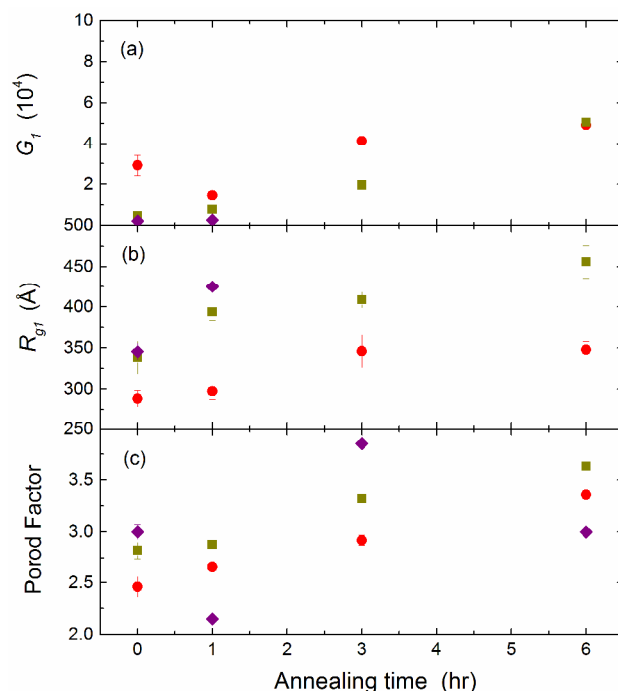
Figure 6. Values for low-q fitting coefficients: (a) amplitude G_1, (b) radius of gyration R_{g1}, and (c) Porod factor P obtained by fitting Eq. 1 to the GISAXS data for the PTB blends shown in Figure 4 as a function of aging time simulated by thermal annealing: (●) PTB4:PCBM, (■) PTB(THP):PCBM, and (♦) dPTB:PCBM.

Values for the parameters describing the low-q terms R_{g1}, G_1 and P are shown in Figs. 6 (a-c). While the accessible q-range at low-q is not sufficient to definitively describe structure larger than 50 nm, the length-scale R_{g1} does provide some information about larger scale structure in both PTB4 and PTB(THP) blends, and indicates structure of roughly 20-40 nm, which grows slightly during aging. The amplitude of this term grows significantly in the PTB(THP) blends with aging but is roughly constant in the PTB4 samples. But in both cases, the contribution of this structure to the scattering, as evidenced in the amplitude G_1, is significantly higher in the PTB4 and PTB(THP) blends than the dPTB samples, consistent with increased phase separation. The increase in the Porod exponent P in these samples indicates that the aggregates become more compact as the samples age.

The results of all three morphological studies, optical microscopy, TEM and GISAXS, demonstrate that the morphology of films made of dPTB:PCBM blends are stable during an accelerated aging process achieved by thermal annealing. Films made of PTB(THP):PCBM,

PTB4:PCBM, and P3HT:PCBM blends all show evidence of the growth of PCBM aggregates. We attribute the stability of films made of dPTB:PCBM blends to the suppression of phase separation in the system. In these films, deprotection is a result of the removal of the THP-terminated pendants; this leads to a reduction in the length of the side chains attached to the PTB backbone. It has been shown that less bulky side chains lead to less phase separation of PCBM and polymer in blends of PTB-related polymers and PCBM.[22] It is also known that shorter side chains rigidify the polymer backbone leading to the better stability in the morphology.[14] Furthermore, the remaining side chain alkyl alcohols are available through hydrogen bonding, which has been shown to rigidify the molecular structure and suppress phase separation.[32]

3. Conclusions

We present a thermo-cleavable polymer that shows stable photovoltaic properties upon cleavage of the THP-attached side chains when used as the active layer in a BHJ photovoltaic cell. Stability was tested by annealing samples for up to 6 hr at 130 °C. Optical microscopy, TEM and GISAXS results show that this can be attributed to a stable morphology at nano and micro length scales. Optical microscopy reveals that P3HT:PCBM, PTB4:PCBM, PTB(THP):PCBM samples all develop micron-sized PCBM aggregates upon aging. In contrast, no such aggregates are observed after thermal cleaving of the THP groups (dPTB:PCBM) over the same time period. TEM and GISAXS results confirm that the morphology of dPTB:PCBM films is stable at the nanoscale as well. GISAXS measurements also show that more uniform blends are obtained with the PTB polymers than the P3HT polymers, as evidenced by smaller PCBM aggregates. We attribute the stability of films made of dPTB:PCBM blends to the suppression of phase separation in the system. While the monomer on which PTB(THP) is built is most similar to that of PTB4, the results should be transferable to other members of the PTB series. In particular, the monomer from this series most widely used in photovoltaic studies, PTB7, also contains a fluorine atom in the thienothiophene unit and differs from PTB4 only in the branching of one of the side chains.

4. Experimental Section

Materials and Synthesis: Chemicals were purchased from Sigma-Aldrich, Alfa Aesar, TCI America, and SunaTech and were used without further purification. All manipulations involving

air-sensitive reagents were performed in an argon atmosphere. PTB4 and 4,8-dihydroxybenzo[1,2-b:4,5-b']dithiophene were prepared according to references [22] and [37], respectively.

Synthesis of BDTTHP. The mixture of 4,8-dihydroxybenzo[1,2-b:4,5-b']dithiophene (1.00 g, 4.50 mmol), 2-(2-bromoethoxy)tetrahydro-2H-pyran (2.35 g, 11.25 mmol), $Na_2CO_3 \bullet H_2O$ (1.67 g, 13.50 mmol), KI (0.20 g, 1.20 mmol), and 2-butanone (40 ml) in a 250 ml of round bottom flask (RBF), was refluxed for about 40 hours under an argon atmosphere, and then concentrated. The product was isolated by dichloromethane/H_2O extraction, dried with $MgSO_4$, filtered, and concentrated. The crude product was purified by a silica gel column (eluent: hexane/ethyl acetate=3:1) to afford a yellow sticky oil (0.8 g, 37.2 %). ^{1}H NMR (500 MHz, CDCl$_3$): δ7.60 (d, 2H), 7.39 (d, 2H), 4.78 (t, 2H), 4.47 (t, 4H), 4.10 (m, 2H), 3.90 (m, 4H), 3.56 (m, 2H), 1.91 (m, 2H), 1.74 (m, 4H), 1.58 (m, 6H).

Synthesis of BDTTHPSn. BDTTHP (0.70 g, 1.46 mmol) and 12 mL of anhydrous tetrahydrofuran were added into a 100 mL of RBF under Ar and then the solution was cooled down to -78 ^{o}C. n-Butyllithium solution (1.46 mL, 3.66 mmol, 2.5 M in hexane) was added dropwise into the flask and the mixture was stirred in an acetone/liquid nitrogen bath for 30 min and then at room temperature for 30 min, and white precipitate was formed in the flask. After cooling the flask to -78 ^{o}C, trimethyltin chloride solution (4.39 mL, 4.39 mmol, 1.0 M in hexanes) was added via a syringe in one portion and the reaction mixture quickly turned clear. The cooling bath was removed and the reaction mixture was stirred overnight at room temperature. The reaction was quenched by pouring into 100 mL of water, extracted with diethyl ether, and dried over anhydrous magnesium sulfate. The organic solvent was removed by rotary evaporation, and then the crude product was purified by silica gel column with eluent of hexanes:ethyl acetate=3:1 and crystallization from ethanol to yield a white solid (0.5 g, 42.4 %). ^{1}H NMR (500 MHz, CDCl$_3$): δ7.63 (s, 2H), 4.79 (t, 2H), 4.49 (t, 4H), 4.09 (m, 2H), 3.90 (m, 4H), 3.55 (m, 2H), 1.95 (m, 2H), 1.77 (m, 4H), 1.61 (m, 6H), 0.45 (s, 18H). ^{13}C NMR (125MHz, CDCl$_3$): δ142.82, 140.70, 134.15, 133.18, 128.13, 98.85, 66.50, 62.01, 30.62, 25.50, 19.36, -8.33.

Synthesis of polymer PTB-THP. Octyl-6-dibromo-3-fluorothieno[3,4-b]thiophene-2-carboxylate (0.1363 g, 0.289 mmol), BDTTHPSn (0.2321 g, 0.289mmol), and Pd(PPh$_3$)$_4$ (4 mol%, 13 mg) were weighted into a 25 mL round-bottom flask. The flask was subjected to three successive cycles of vacuum followed by refilling with argon. Then, anhydrous N,N-

dimethylformamide (DMF, 1 mL) and anhydrous toluene (5 mL) were added via a syringe. The polymerization was carried out at 120 °C for 20 h under Argon protection. The raw product was precipitated into methanol and collected by filtration. The precipitate was extracted with acetone and further with hexane. The residue was then extracted into chloroform to afford 0.18 g (79.3 % yield) of dark purple solid. ^{1}H NMR (500 MHz, CD$_2$Cl$_2$): δ 7.70-7.00 (2H, br), 5.00-3.00 (16H, br), 2.50-0.70 (27H, br). GPC: Mn (10.5 × 10^3 g/mol), PDI (2.82).

Characterization. ^{1}H and ^{13}C NMR spectra were recorded on a Bruker DRX-500 spectrometer, and referenced to tetramethylsilane. The molecular weight was obtained with a Waters model 1515 GPC (gel permeation chromatograph) in THF with a calibration curve prepared from polystyrene standards. TGA analysis was performed at 10 °C/min with 5 - 8 mg of polymer sample under N$_2$ using a HiRes TGA 2950 Thermogravimetric Analyzer (TA Instruments). The onset temperature was estimated from the point of intersection of two lines: one extrapolated from the slope of the curve just prior to loss of the THP group and the second from the steepest part of the curve. FTIR spectra were recorded using a Bomem Michelson FTIR (120 series). PTB-THP and its mixture with 5 mol-% of camphorsulfonic acid (CSA) in chloroform were drop-cast separately onto sodium chloride disks. The film of PTB-THP with CSA was heated at 150 ℃ for 5 min and rinsed with acetonitrile to remove the residues of CSA. UV-vis absorption spectra were measured using a Cary 300 Bio (Varian) spectrophotometer. Film thicknesses were measured by an Alpha-Step IQ® surface profiler. DSC measurements were made on 3.45 mg of PTB(THP) powder at a scanning rate of 10 ^{o}C/min. Cyclic voltammetry (CV) measurements were carried out in 0.1 mol·L^{-1} tetrabutylammonium tetrafluoroborate (Bu$_4$NBF$_4$) acetonitrile solution under inert N$_2$ atmosphere, with the polymer-coated glassy carbon as the working electrode, a platinum wire as the counter electrode, and a saturated calomel electrode as the reference electrode. The scan rate was set to 50 mV/s. The potential of ferrocene/ferrocenium (Fc/Fc$^+$) was found at 0.4 V under the same experimental conditions as a calibration. It is reported that the redox potential of Fc/Fc$^+$ has an absolute energy level of -4.80 eV in vacuum.[38] Therefore the energy levels of the polymer are calculated from $E = e\,(-4.4 - \varphi)\,V$, where E is the absolute energy level to vacuum, and φ is the corresponding potential measured with CV.

Sample Preparation: Polymer blend films were made from stock solutions which consisted of 10 mg polymer, 10 mg PC$_{61}$BM and either 0.5 mL 1,2 dichlorobenzene (DCB) and 0.5 mL of

chloroform (for PTB(THP):PCBM and P3HT:PCBM blends) or 1 mL of DCB (PTB4:PCBM blends). The mixtures were stirred overnight at room temperature to ensure thorough mixing. dPTB samples were prepared for cleaving by adding 0.15 mL of a 5 mol% solution of CSA in tetrahydrofuran (THF). The stock solutions as well as films for PV measurements and morphology characterization were prepared in a nitrogen-filled glove box (O_2 and H_2 levels ≤ 0.1 ppm).

PV Device Fabrication and Measurements. ITO-coated glass slides (2.0 x 1.0 cm^2) were ultrasonically cleaned in isopropyl alcohol, acetone, deionized $H_2O:H_2O_2:NH_4OH$ (5:1:1 vol. ratio), deionized H_2O, and acetone. 35 nm of poly(ethylene dioxythiophene): polystyrenesulfonate (PEDOT:PSS) (Heraeus Materials Technology) was spin-cast onto the ITO, annealed at 140 °C under air for 10 min in a pre-heated oven, and immediately transferred into a glove box. Subsequently, the active layer of polymer:PC$_{61}$BM in the weight ratio of 1:1 with or without 5 mol% of CSA was spin-cast from dichlorobenzene. To cleave THP groups, the active films with CSA were heated to 150 °C for 5-10 min in a glove-box filled with N_2. ~20 nm of Ca followed by ~80 nm of Al were thermally evaporated under at $< 1 \times 10^{-8}$ Torr through a shadow mask. After film formation and deprotection, the films were rinsed with acetonitrile for 1 min to remove CSA before device testing. The active area of the device was around 0.30 cm^2; the thickness of the active layer was 80 nm. The current density-voltage (J-V) curves were measured using a Keithley 2400 source meter under a Newport 300W Xenon arc lamp source. EQE measurements were conducted using Corner Stone 260 monochrometer equipped with low power photodetector 841-PE.

Sample preparation for microscopy and scattering. Silicon substrates were ultra-sonicated at 40 °C in hexane for 15 min, deionized water for 5 min, isopropanol for 15 min, and again in deionized water for 5 min. PEDOT:PSS was spin-cast at 5000 rpm onto the cleaned silicon substrate. The substrates were then annealed for 10 min in a preheated oven at 140 °C and subsequently stored in the glove. The polymer blend solutions were spin-cast on the PEDOT:PSS-coated substrates at 1000 rpm for 1 min and left inside the glove box overnight to dry (as-cast films). Films were annealed at 130 °C. Because 5 min of thermal treatment is required to cleave the PTB(THP) and convert it to dPTB, and to maintain consistency of sample preparation, the first annealing step for all samples involved placing them on a hot plate in the glove box for 5 min at 130 °C. These samples are labeled as having been aged for 0 hr. Samples

were subsequently annealed for either 1, 3 or 6 hr at this temperature. The resulting samples are referred to as having been aged for 1, 3 and 6 hr. TEM samples were obtained by soaking the sample-coated substrate in deionized water, which dissolves PEDOT:PSS and releases the film, which was then picked up on a 200 mesh copper grid.

Morphological Characterization:

Optical Microscopy. A Zeiss Axio microscope equipped with AxioCam MRc 5 camera was used for optical microscopy.

Transmission Electron Microscopy. A Hitachi 8100 and a Technai Osiris were used for TEM.

GISAXS Measurements. GISAXS measurements were carried out at the Canadian Light Source (CLS) on beamline 06ID-1 for Hard X-ray Micro-Analysis (HXMA). A photon energy of 8.979 KeV was used. Samples were placed on a horizontal stage inside a vacuum chamber. Measurements were made at an angle of incidence of 0.16^{o} and data was recorded on a Mar165 image plate detector. The Nika data reduction package was used for data reduction.[39] The intensity scattered in the plane parallel to the film was obtained by averaging a stripe of data along the q_y axis at the position of the specular beam over a width of 10 pixels.

References

[1] M. A. Green, K. Emery, Y. Hishikawa, W. Warta, and E. D. Dunlop, *Prog. Photovolt: Res. Appl.* 2015, 23, 1–9.

[2] M. A. Brady, G.M. Su and M. L. Chabinyc, *Soft Matter*, 2011, 7, 11065–11077.

[3] M. Jorgensen, K. Norrman, S. A. Gevorgyan, T. Tromholt, B. Andreasen and F. C. Krebs, *Adv. Mater.* 2012, 24, 580-612.

[4] B. C. Thompson and J. M. J. Frechet, *Angew. Chem. Int. Ed.* 2008, 47, 58-77.

[5] X. Yang and J. Loos, *Macromolecules*, 2007, 40, 1353-1362.

[6] A. J. Moule and K. Meerholz, *Adv. Mater.,* 2008, 20, 240-245.

[7] F. Piersimoni, G. Degutis, S. Bertho, K. Vandewal, D. Spoltore, T. Vangerven, J. Drijkoningen, M. K. Van Bael, A. Hardy, J. D'Haen, W. Maes, D. Vanderzande, M. Nesladek and J. Manca, *J. Polym. Sci. B Polym. Phys.,* 2013, 51, 1209-1214.

[8] S. Ebadian, B. Gholamkhass, S. Shambayati, S. Holdcroft and P. Servati, *Sol. Energ. Mat. Sol. Cells*, 2010, 94, 2258-2264.

[9] M. T. Rispens, A. Meetsma, R. Rittberger, C. J. Brabec, N. S. Sariciftci and J. C. Hummelen, *Chem. Commun.*, 2003, 2116-2118.

[10] M. A. Ruderer, S. Guo, R. Meier, H.-Y. Chiang, V. Korstgens, J. Wiedersich, J. Perlich, S. V. Roth and P. Muller-Buschbaum, *Adv. Funct. Mater*, 2011, 21, 3382-3391.

[11] C.-M. Liu, Y.-W. Su, J.-M. Jiang, H.-C. Chen, S.-W. Lin, C.-J. Su, U-S. Jeng and K.-W. Wei, *J. Mater. Chem. A*, 2014, 2, 20760-20769.

[12] B. J. Kim, Y. Miyamoto, B. Ma and J. M. J. Frechet, *Adv. Funct. Mater.*, 2009, 191, 2273-2281.

[13] B. Gholamkhass and S. Holdcroft, *Chem. Mater.*, 2010, 22, 5371-5376.

[14] F. C. Krebs, H. Spanggaard, *Chem. Mater.,* 2005, 17, 5235-5237.

[15] S. A. Gevorgyan and F. C. Krebs, *Chem. Mater.* 2008, 20, 4386-4390.

[16] J. L. Brusso, M. R. Lilliedal and S. Holdcroft, *Polym. Chem.*, 2011, 2, 175-180.

[17] T, Ameri, G. Dennler, C. Lungenschmied and C. J. Brabec, *Energy Environ. Sci*., 2009, 2, 347-363.

[18] L. Lu and L. Yu, *Adv. Mat.*, 2014, 26, 4413-4430.

[19] J. M. Szarko, J. Guo, Y. Liang, B. Lee, B. S. Rolczynski, J. Strzalka, T. Xu, S. Loser, T. J. Marks, L. Yu and Lin X. Chen, *Adv. Mat.*, 2010, 22, 5468-5472.

[20] L. Derue, Ol, Dautel, A. Tournebize, M. Drees, H. Pan, S. Berthumeyrie, B. Pavageau, E. Cloutet, S. Chambon, L. Hirsch, A. Rivaton, P. Hudhomme, A. Facchetti and G. Wantz, *Adv. Mater.* 2014, 26, 5831-5838.

[21] H. C. Wong, Z. Li, C. H. Tan, H. Zhong, Z. Huang, H. Bronstein, I. McCulloch, J. T. Cabral and J. R. Durrant, *ACS Nano*, 2014, 8, 1297-1308.

[22] Y. Liang, D. Feng, Y. Wu, S.-T. Tsai, G. Li, C. Ray and L. Yu, *J. Am. Chem. Soc.*, 2009, 131, 7792-7799.

[23] J. Yu, M. Abley, C. Yang and S. Holdcroft, *Chem. Commun.* 1998, 15, 1503-1504.

[24] J. Yu and S. Holdcroft, *Chem. Mater.,* 2002, 14, 3705-3714.

[25] C. J. Brabec, A. Cravino, D. Meissner, N. S. Sariciftci, T. Fromherz, M. T. Rispens, L. Sanchez, and J. C. Hummelen, *Adv. Funct. Mater.*, 2001, 11, 374-380.

[26] M. Campoy-Quiles, T. Ferenczi, T. Agostinelli, P. G. Etchegoin, Y. Kim, T. D. Anthopouls, P. N. Stavrinou, D. D. C. Bradley and J. Nelson, *Nature Materials,* 2008, 7, 158-164.

[27] V. Turkovic, S. Engmann, G. Gobsch and H. Hoppe, *Synt. Met.*, 2012, 161, 2534-2539.

[28] F. Machui and C. J. Brabec, in *Semiconducting Polymer Composites: Principles, Morphologies, Properties and Applications*, edited by X. Yang (Wiley-VCH Verlag GmbH & Co., 2012), Ch. 1.

[29] D. M. DeLongchamp, R. J. Kline and A. Herzing, *Energy Environ. Sci.,* 2012, 5, 5980-5993.

[30] M.-Y. Chiu, U-S. Jeng, C.-H. Su, K. S. Liang and K.-H. Wei, *Adv. Mater.*, 2008, 20, 2573-2578.

[31] W.-R. Wu, U-S. Jeng, C.-J. Su, K.-H. Wei, M.-S. Su, M.-Y. Chiu, C.-Y. Chen, W.-B. Su, C.-H. Su and A.-C. Su, *ACS Nano*, 2011, 5, 6233–6243.

[32] J. W. Kiel, A. P. R. Eberle and M. E. Mackay, *Phys. Rev. Lett.*, 2010, 105, 168701.

[33] P. Vahdani (201x), Ph.D. thesis, Simon Fraser University.

[34] G. Beaucage, *J. Appl. Cryst.*, 1996, 29, 134-146.

[35] J. Ilavsky and P. R. Jemian, *J. Appl. Cryst.*, 2009, 42, 347-353.

[36] J. Yu, F. P. Orfino and S. Holdcroft, *Chem. Mater.*, 2001, 13, 526-529.

[37] D. Lee, S. W. Stone and J. P. Ferraris, *Chem. Commun.*, 2011, 47, 10987-10989.

[38] J. Pommerehne, H. Vestweber, W. Guss, R. F. Mahrt, H. Bassler, M. Porsch, J. Daub, *Adv. Mater.* 1995, 7, 551-554.

[39] J. Ilavsky, *J. Appl. Cryst.*, 2012, 45, 324-328.